Thermodynamic coarsening arrested by viscous fingering in partially miscible binary mixtures

Xiaojing Fu, Luis Cueto-Felgueroso, and Ruben Juanes

Phys. Rev. E **94**, 033111 — Published 20 September 2016

DOI: 10.1103/PhysRevE.94.033111

Thermodynamic coarsening arrested by viscous fingering in partially-miscible binary mixtures

Xiaojing Fu,[1] Luis Cueto-Felgueroso,[1,2] and Ruben Juanes[1,*]

[1]*Massachusetts Institute of Technology, 77 Massachusetts Ave, Building 1, Cambridge, Massachusetts 02139, USA*
[2]*Technical University of Madrid, Calle del Profesor Aranguren 3, 28040 Madrid, Spain*

(Dated: September 1, 2016)

We study the evolution of binary mixtures far from equilibrium, and show that the interplay between phase separation and hydrodynamic instability can arrest the Ostwald ripening process characteristic of non-flowing mixtures. We describe a model binary system in a Hele-Shaw cell using a phase-field approach with explicit dependence of both phase fraction and mass concentration. When the viscosity contrast between phases is large (as is the case for gas and liquid phases), an imposed background flow leads to viscous fingering, phase branching and pinch-off. This dynamic flow disorder limits phase growth and arrests thermodynamic coarsening. As a result, the system reaches a regime of statistical steady state in which the binary mixture is permanently driven away from equilibrium.

PACS numbers: 47.55.N-, 47.15.gp, 47.20.Gv, 47.51.+a

Spinodal decomposition is the process by which a thermodynamically unstable mixture separates into two phases. The signature feature of this process is coarsening: the characteristic length scale of phase separation grows algebraically with time [1–3]. Thermodynamic coarsening—first studied in the context of solid alloys [2, 4]—can be fundamentally altered in fluid mixtures by means of hydrodynamic effects that lead to more complex dynamics. For instance, hydrodynamic coalescence due to curvature-induced pressure differences can enhance the coarsening rate [5, 6]. Under uniform shear flow, a highly anisotropic layered phase ordering appears in the mixture [7–9]. Under turbulent flow, experiments [10, 11] and numerical simulations [12, 13] have shown that coarsening is suppressed due to vigorous stirring, a result that is also observed when a chaotic flow is imposed [14].

These observations arise from the coupling of a phase-ordering process (promoting coarsening) to a velocity field with *externally imposed* strong disorder (suppressing coarsening) [14]. The paradigmatic model used to investigate this process is the advective Cahn–Hilliard equation coupled to the incompressible Navier–Stokes equations [12–15]. In this case, the Navier–Stokes equations contain a capillary term that embodies gradients in chemical potential, and thereby a feedback from the phase-evolution equation. This term alone, however, is insufficient to suppress coarsening—on the contrary, the main observation is that, in an unstirred fluid, domain growth of the phase-separating field is enhanced [12].

In this letter, we set to elucidate whether thermodynamic coarsening can be arrested by the coupling between phase-ordering and hydrodynamics in the absence of external mechanical forcing. We study spinodal decomposition of a binary fluid mixture driven by Darcy flow, such as flow in a Hele-Shaw cell (a thin gap between two parallel plates) or porous media. Our interest is in systems that naturally phase-separate into phases of very different viscosity (as is typical of liquids and gases). Under these conditions, two relevant effects set in. On one hand, there is strong feedback between phase ordering and fluid velocity via a phase-dependent mixture viscosity. On the other, the well-known viscous fingering hydrodynamic instability [16–19] induces phase branching, splitting and pinch-off [20–22]. While many aspects of viscous fingering have been studied—including its role on fluid mixing [23–25] and ensuing chemical reactions [26–28]—its impact on phase separation of a fluid mixture remains unexplored.

A complicating factor in fluid binary mixtures is that miscibility can change appreciably with the ambient conditions, which often introduces compositional effects to two-phase problems. In previous studies of spinodal decomposition coupled to flow, fluid phase is inferred from composition, and not independently described [6, 9, 12–15]. The free energy of such mixtures is formulated as a functional of molar fractions and their gradients and, in its simplest setting, the coarsening dynamics is described by a Cahn–Hilliard equation [29]. Here, in contrast, we consider *partially miscible* systems—components can exchange between the two phases and, therefore, fluid concentrations evolve independently from the phase variable. During spinodal decomposition, our mixture phase-separates into domains with different compositions, accompanied by redistribution of composition between phases. Describing such mixture requires having separate evolution equations for phase and concentration, and defining a free energy that is a function of both variables. Analogous two-field approaches have been extensively adopted in the simulation of solidification of binary alloys [30–33]. By adopting this more general framework, we investigate the two-way coupling between thermodynamics (compositional phase behavior and phase ordering) and hydrodynamics (viscously unstable Darcy flow), and find that the system reaches a statistical steady state in which viscous fingering not only arrests phase growth, but also drives the mixture away from compositional equilibrium permanently.

Without loss of generality, we study a binary mixture representative of a CO_2–water system. The two fluids, which we denote *gas* (g) and *liquid* (l), have different viscosities, $\mu_l \gg \mu_g$. When in contact, the two-component system naturally evolves towards compositional equilibrium through mutual component exchange, resulting in a CO_2-rich gas phase

and a water-rich liquid phase. We introduce two variables defined point-wise in the domain: the gas volume fraction, ϕ, and the CO_2 molar fraction, c. Within a vapor bubble, ϕ=1; within the liquid phase, ϕ=0.

We adopt a phase-field modeling approach, which has proved effective at describing immiscible two-phase flow in confined geometries like Hele-Shaw [22, 34–41] or porous media [42]. Our model describes incompressible, isothermal, two-phase flow with two-component transport in a Hele-Shaw cell. The gap-averaged dimensionless governing equations are:

$$\nabla \cdot \mathbf{u} = 0, \quad \mathbf{u} = -\frac{1}{\mu(\phi)}\nabla P, \tag{1}$$

$$\frac{\partial \phi}{\partial t} + \nabla \cdot (\mathbf{u}\phi) + \frac{1}{\mathrm{Ca}}\lambda \frac{\delta F}{\delta \phi} = 0, \tag{2}$$

$$\frac{\partial c}{\partial t} + \nabla \cdot (\mathbf{u}c) - \frac{1}{\mathrm{Pe}}\nabla \cdot \left[\lambda \nabla \left(\frac{\delta F}{\delta c}\right)\right] = 0. \tag{3}$$

Equations (1) are the continuity equation for an incompressible mixture, where $\mathbf{u}$ is the mixture velocity described by Darcy's law, P is a kinematic pressure, and μ is the mixture viscosity, assumed to follow an exponential dependence on phase fraction, μ=$\mu_g \exp(R(1-\phi))$, where R=$\log(\mu_l/\mu_g)$ is the viscosity contrast.

Under the context of phase-field modeling, we understand ϕ also as a phase variable that interpolates smoothly between the two bulk phases over a well-resolved, diffuse interface. Time evolution of ϕ simulates gas dissolution/exsolution [Eq. (2)]. In the presence of flow, it is a relaxation process towards a minimum of a free energy functional, $F(\phi, c, \nabla\phi, \nabla c)$ [43]. The direction of steepest energy descent, obtained by taking the variational derivative of F with respect to ϕ, $\delta F/\delta\phi$=$\partial F/\partial\phi - \nabla\cdot[\partial F/\partial(\nabla\phi)]$, drives phase transformation under Allen–Cahn dynamics [44]. In Eq. (2), Ca=$(u_c b)/(\lambda_c \epsilon_\phi^2 T/b^2)$ plays the role of a capillary number—ratio between time scales associated with phase change and advection—where u_c is the characteristic flow velocity, λ_c the characteristic mobility, T the temperature, b the gap thickness, $\epsilon_\phi^2 T/b$ is the interfacial tension, and λ=$0.01+c(1-c)$ is the regularized dimensionless mobility. The evolution of c is described by a nonlinear advection–diffusion equation Eq. (3), where the component diffusion is driven by gradients in chemical potential, $\Psi \equiv \delta F/\delta c = \partial F/\partial c - \nabla\cdot[\partial F/\partial(\nabla c)]$. In Eq. (3), Pe=$(u_c b)/(\lambda_c \omega_{\mathrm{mix}} T)$ plays the role of a Péclet number—ratio between rate of advection and diffusion—where $\omega_{\mathrm{mix}} T$ is the energy (per unit volume) associated with mixing.

The free energy functional, F, plays a central role in the thermodynamic behavior our binary mixture. Following the classical Cahn–Hilliard formulation for a binary system [29], our F subsumes interfacial and bulk energy contributions:

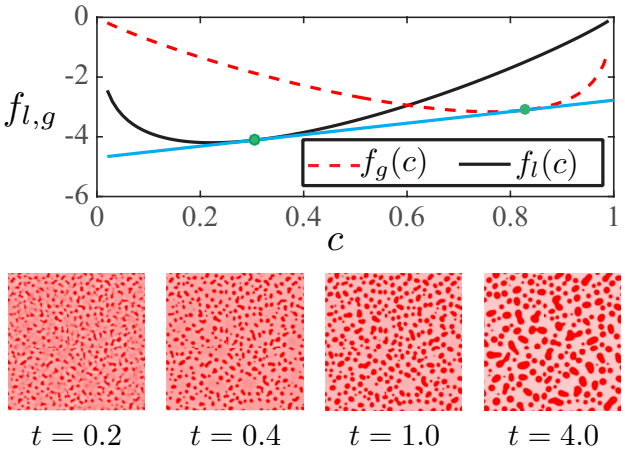

FIG. 1. (Top) The common tangent construction (blue line) on the bulk free energy of pure phases yields the equilibrium concentrations (green circles) within gas and liquid. For parameters α_l=1, β_l=500, α_g=200, β_g=2×10^{-4}, the equilibrium compositions are c_l^{eq}≈0.304 and c_g^{eq}≈0.828. (Bottom) Zoomed-in snapshots of c illustrate the process of spinodal decomposition of a domain that is initially filled with supersaturated liquid (t=0). The progression shows vapor bubbles (high c, red-colored) that nucleate and coarsen out of the liquid phase (low c, pink-colored).

$$F(\phi, c, \nabla\phi, \nabla c) = \int_V \left\{ \frac{1}{2}(\nabla\phi)^2 + \epsilon\frac{1}{2}(\nabla c)^2 + \frac{1}{\mathrm{Ch}}W(\phi) + \frac{1}{\mathrm{Ma}}\left[f_l(c)(1-g(\phi)) + f_g(c)g(\phi)\right] \right\} dV. \tag{4}$$

The first two terms in Eq. (4) capture the interfacial energy associated with phase and compositional boundaries. The characteristic interfacial energy per unit volume associated with ϕ and c are $\epsilon_\phi^2 T$ and $\epsilon_c^2 T$ respectively. We introduce ϵ=$\epsilon_c^2/\epsilon_\phi^2$ as the ratio between the two energy scales. The third term is the part of the bulk free energy responsible for phase separation, where $W(\phi)$=$\frac{1}{4}\phi^2(1-\phi)^2$ adopts the shape of a double-well, determining the two stable states of W: ϕ=0 or ϕ=1. The parameter Ch=$(\epsilon_\phi^2/b)/\omega$ is the Cahn number, where ωT is the energy (per unit volume) associated with the double-well energy. The last term, known as the bulk mixing energy, is the part of the bulk free energy responsible for partially miscible behavior; it scales with the inverse of Ma=$(\epsilon_\phi^2/b)/\omega_{\mathrm{mix}}$, which plays the role of a solutal Marangoni number. We adopt a form for mixing energy that is commonly used in the field of binary alloy solidification [30], where the energy is an interpolation in ϕ between liquid and gas excess energies (f_l and f_g), which are functions of c only. The interpolation function $g(\phi)$=$-\phi^2(2\phi-3)$ satisfies that the system approaches the stable states ϕ=$\{0,1\}$ with zero slope, which ensures positivity of the phase variable [30]. The excess free energy of each phase are due to compositional effects; here we adopt the Wilson model [45]: $f_l(c)$=$c\log c$+$(1-c)\log(1-$

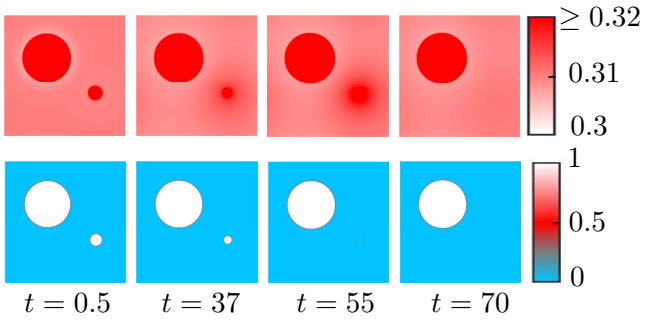

FIG. 2. Snapshots of c (top) and ϕ (bottom) illustrating the Ostwald ripening process in a system with a small and a large vapor bubble, in an liquid bath that is initially at local equilibrium.

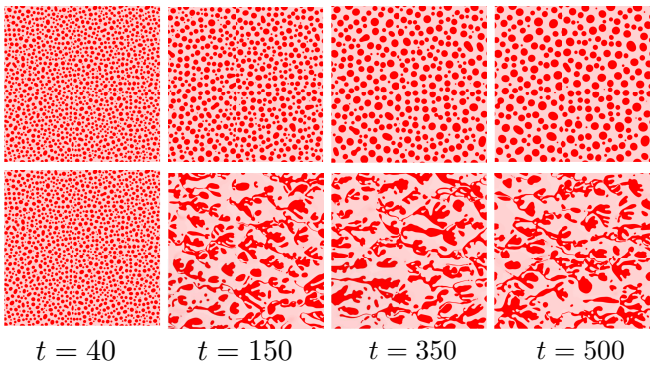

FIG. 3. Snapshots of c at t=40, 150, 350 and 500, under no flow (top) and with periodic left-to-right flow imposed at t>40 (bottom). See Video 1 [50].

$c)-c\log(c+\alpha_l(1-c))-(1-c)\log(1-c+\beta_l c)$ for the liquid, and $f_g(c)=c\log c+(1-c)\log(1-c)-c\log(c+\alpha_g(1-c))-(1-c)\log(1-c+\beta_g c)$ for the gas. The equilibrium concentrations within each phase are then obtained by the common tangent construction of f_l and f_g [3, 46] (Fig. 1, top).

We conduct high-resolution numerical simulations of this compositional phase-field model. We solve Eqs. (1)–(3) sequentially: first obtaining the velocity using the streamfunction-vorticity formulation [47, 48]; then updating c and ϕ using a Fourier pseudo-spectral discretization and using a biharmonic-modified time stepping [49]. Our simulations are on a bi-periodic square domain of size 160×160 and parameter values Ca=2, Pe=128, Ch=$1/400$, Ma=$1/40$ and ϵ=8 (and parameters of the Wilson model given in Fig. 1, top). The domain is initially filled with liquid phase that is supersaturated: $\phi(x,y,t{=}0){=}0$, $c(x,y,t{=}0){=}0.36\pm0.1$. We perturb the initial concentration field with random uncorrelated noise to promote nucleation of gas bubbles. The supersaturated liquid is thermodynamically unstable and undergoes spinodal decomposition almost immediately, where the domain phase-separates into vapor bubbles surrounded by liquid (Fig. 1, bottom).

Ostwald ripening is an out-of-equilibrium process in which large phase domains grow at the expense of smaller ones, by virtue of minimizing interfacial energy [2, 4]. To illustrate the ability of our model to reproduce this well known phenomenon, we simulate two vapor bubbles of different sizes in a liquid bath, and initialize the system to be at compositional equilibrium locally within each phase: $c_l{=}c_l^{\rm eq}$, $c_g{=}c_g^{\rm eq}$ (Fig. 2). Despite the initial local-equilibrium configuration, the smaller bubble dissolves into the liquid phase, leaving a patch of excess concentration that diffuses into the larger bubble, expanding its size (the larger bubble, in turn, develops a rim of undersaturated liquid around it). Over the entire process, the total gas volume fraction in the domain is unchanged.

It is well known that, as a result of Ostwald ripening, an initially nucleated domain will coarsen continuously (Fig. 3, top; see Video 1 [50]) until it consists of a single large bubble (not shown here), thereby minimizing the system's interfacial energy and chemical potential gradients. Here, we define r as the square root of the area of an individual vapor bubble. We obtain information on individual bubbles through image segmentation of the ϕ-field and compute $\langle r\rangle$ as the average length scale associated with a given domain image. We find a power-law scaling of the coarsening dynamics: $\langle r\rangle\sim t^{1/3}$ (Fig. 4a), indicative of diffusive-growth regime. The bubble-size distribution, $f(r)$, is time-independent when scaled by $\langle r\rangle$ (Fig. 4b). Both observations are in agreement with the Lifshitz–Slyozov–Wagner theory [51–54] of Ostwald ripening in 2D. We have confirmed with additional simulations (not shown here) that the power-law scaling holds for other values around Ma $=1/40$, when the system is still dominated by interfacial dynamics. In the limit of Ma $\to 0$, the mixture behaves as fully miscible, and the LSW theory does not apply.

Given the ability of our model to simulate thermodynamic coarsening, we now turn our attention to the impact of hydrodynamics on the coarsening process. To investigate this effect, we perform a simulation that is identical to the one just described, but introducing periodic left-to-right background flow with unit velocity at t>40 (Fig. 3, bottom; see Video [50]). The unfavorable viscosity contrast between liquid and gas (μ_l/μ_g=20.9) leads to viscous fingering, a hydrodynamic instability when a low-viscosity fluid displaces a high-viscosity fluid [16–19]. This leads to phase branching and tip splitting [20, 21], which in our case destabilize the leading edge of gas bubbles and induce pinch-off events [22, 39]. As a result, vapor bubbles undergo persistent breakup and coalescence. The dynamic disorder in the phase field feeds back to the flow field through a phase-dependent viscosity Eq. (1), leading to the intrinsic emergence of a dynamic and highly heterogeneous flow field. By virtue of this interplay, coarsening is arrested immediately, and the system enters a statistical steady state characterized by a relatively constant arrest length scale (Fig. 4a) and a time-independent bubble-size distribution $f(r)$; the new distribution is more skewed, featuring a dominant presence of smaller-than-average bubbles (Fig. 4c). We have confirmed with additional simulations (not shown here) that the emergence of an arrest length scale is not observed in a fully miscible system under similar flow dynamics [23], and that the effect of Korteweg stress [55, 56] alone is

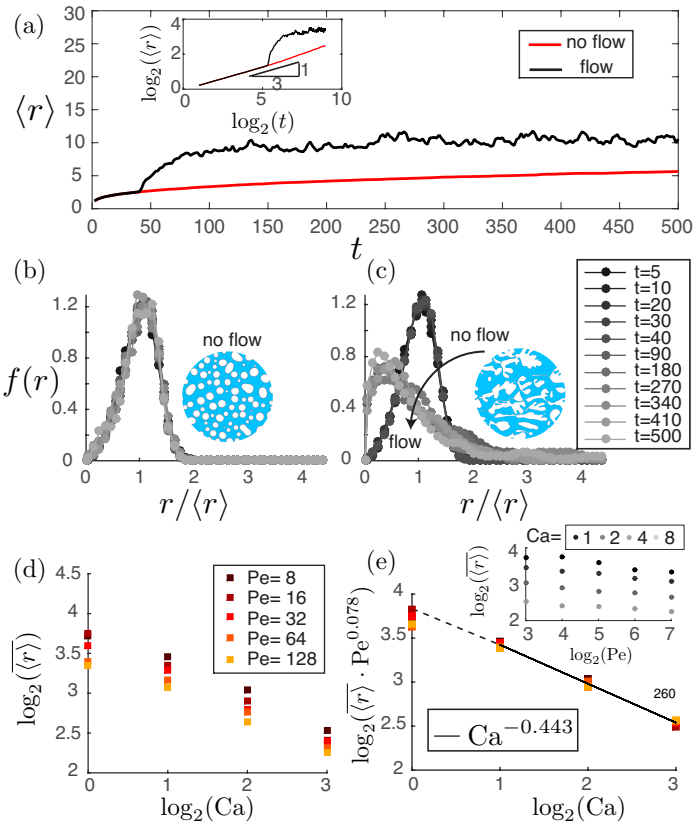

FIG. 4. (a) $\langle r \rangle^3$ vs. t for simulations without flow (dashed red line) and with background flow after $t = 40$ (solid black line), emphasizing arrest of thermodynamic coarsening in the presence of flow. Inset: $\langle r \rangle$ vs. t in log-log scale, emphasizing algebraic growth of spinodal decomposition ($\langle r \rangle \sim t^{1/3}$) in the absence of flow. (b–c) Normalized distribution of $r/\langle r \rangle$ at sampling times for simulations without flow (b) and with flow introduced at $t = 40$ (c). (d) $\overline{\langle r \rangle}$ vs. Ca for different Pe. (e) $\overline{\langle r \rangle}$ rescaled with $\mathrm{Pe}^{-0.078}$ vs. Ca. Inset: $\overline{\langle r \rangle}$ vs. Pe for different Ca.

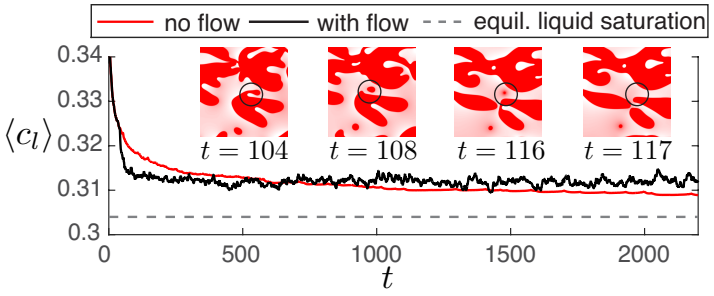

FIG. 5. Evolution of the averaged liquid-phase concentration $\langle c_l \rangle$ for systems without background flow (red solid line) and with background flow after t=40 (black solid line). The gray dashed line indicates equilibrium liquid-phase concentration from the common tangent construction [Fig. 1(top)]. Insets: zoomed-in snapshots of c. The circle highlights pinch-off of a small bubble that quickly dissolves into the liquid—the colormap range is $(0.3, 0.35)$ to emphasize concentration variations around the c_l^{eq}; see Video 2 [50].

insufficient to retain an arrest length scale in fully miscible mixtures.

We study the dependence of the emerging characteristic arrest length scale $\overline{\langle r \rangle}$ (time-averaged $\langle r \rangle$ during the statistical steady state) on Ca and Pe. The fundamental observation is the strong power-law decay of $\overline{\langle r \rangle}$ with Ca, and a weaker decay with Pe (Fig. 4d). Filtering the dependence $\sim \mathrm{Pe}^{-0.078}$ (Fig. 4e, inset) allows us to robustly collapse the data as a function of Ca, $\overline{\langle r \rangle} \sim \mathrm{Ca}^{-0.443}$ (Fig. 4e). This power-law behavior indicates that in the regime dominated by interfacial dynamics (Ca>1), the dependence of the emerging length scale on Ca is congruent with the one predicted by linear stability analysis of classical immiscible viscous fingering, $\sim \mathrm{Ca}^{-0.5}$ [19]. We postulate that the discrepancy in the observed exponents is due to thermodynamic coarsening effects.

The interplay between the hydrodynamic instability (viscous fingering) and thermodynamic coarsening (Ostwald ripening) in partially miscible mixtures turns out to have surprising macroscopic consequences. Let $\langle c_l \rangle = \iint c(1-\phi)dxdy / \iint (1-\phi)dxdy$ be the domain-averaged liquid phase concentration and compare $\langle c_l \rangle$ vs. t for both simulations (Fig. 5). In the absence of background flow, $\langle c_l \rangle$ approaches the theoretical saturation of $c_l^{\mathrm{eq}} \approx 0.304$ from the initial supersaturation level of $\langle c_l \rangle = 0.36$. The ultimate steady state, where $\langle c_l \rangle = c_l^{\mathrm{eq}}$, is only reached when Ostwald ripening culminates the coarsening process in a single vapor bubble (not shown here). Under background flow, in contrast, the approach towards compositional equilibrium is interrupted as soon as flow is introduced, and $\langle c_l \rangle$ fluctuates about a steady state value that, surprisingly, is above the local-equilibrium concentration: $\langle c_l \rangle \approx 0.312 > c_l^{\mathrm{eq}}$.

We propose the following mechanism to explain the observed supersaturation in the liquid (Fig. 5, insets; see Video 2 [50]). The viscous instability leads to recurrent pinch-off of small bubbles from large patches of vapor. A newly formed small bubble is quickly consumed by surrounding larger bubbles due to Ostwald ripening. This is achieved, as shown in Fig. 2, by small bubbles first dissolving into the liquid. The mass transfer into large bubbles is limited by diffusion, implying that if the rate of bubble shedding is large compared with the rate of diffusive mass transfer through the liquid, this disparity will result in an excess dissolved concentration. Therefore, the interplay between hydrodynamic instability and thermodynamic coarsening results in a liquid phase that is, on average, always supersaturated. In other words, the emergence of flow disorder from viscous fingering drives the mixture out of compositional equilibrium permanently.

This work was funded by the US Department of Energy (CAREER Award DE-SC0003907, and grants DE-SC0009286 and DE-FE0013999). LCF acknowledges a 'Ramon y Cajal' Fellowship from the Spanish Ministry of Economy and Competitiveness (RYC-2012-11704).

* juanes@mit.edu

[1] H. Furukawa, Adv. Phys. **34**, 703 (1985).
[2] P. W. Voorhees, Annu. Rev. Mater. Res. **22**, 197 (1992).
[3] A. J. Bray, Adv. Phys. **43**, 357 (1995).
[4] W. Ostwald, Zeit. fur Physik Chemie **34**, 495 (1900).
[5] E. D. Siggia, Phys. Rev. A **20**, 595 (1979).
[6] A. J. Wagner and J. M. Yeomans, Phys. Rev. Lett. **80**, 1429 (1998).
[7] K. Y. Min and W. I. Goldburg, Phys. Rev. Lett. **70**, 469 (1993).
[8] T. Hashimoto, K. Matsuzaka, E. Moses, and A. Onuki, Phys. Rev. Lett. **74**, 126 (1995).
[9] Z. Shou and A. Chakrabarti, Phys. Rev. E **61**, 2200 (2000).
[10] D. J. Pine, N. Easwar, J. Maher, and W. Goldburg, Phys. Rev. A **29**, 308 (1984).
[11] P. Tong, W. Goldburg, J. Stavans, and A. Onuki, Phys. Rev. Lett. **62**, 2668 (1989).
[12] S. Berti, G. Boffetta, M. Cencini, and A. Vulpiani, Phys. Rev. Lett. **95**, 224501 (2005).
[13] P. Perlekar, R. Benzi, H. J. Clercx, D. R. Nelson, and F. Toschi, Phys. Rev. Lett. **112**, 014502 (2014).
[14] L. Berthier, J.-L. Barrat, and J. Kurchan, Phys. Rev. Lett. **86**, 2014 (2001).
[15] R. Ruiz and D. Nelson, Phys. Rev. A **23** (1981).
[16] P. G. Saffman and G. I. Taylor, Proc. R. Soc. Lond. A **245**, 312 (1958).
[17] L. Paterson, J. Fluid Mech. **113**, 513 (1981).
[18] J. V. Maher, Phys. Rev. Lett. **54**, 1498 (1985).
[19] G. M. Homsy, Annu. Rev. Fluid Mech. **19**, 271 (1987).
[20] A. Arnéodo, Y. Couder, G. Grasseau, V. Hakim, and M. Rabaud, Phys. Rev. Lett. **63**, 984 (1989).
[21] E. Lajeunesse and Y. Couder, J. Fluid Mech. **419**, 125 (2000).
[22] L. Cueto-Felgueroso and R. Juanes, J. Fluid Mech. **758**, 522 (2014).
[23] B. Jha, L. Cueto-Felgueroso, and R. Juanes, Phys. Rev. Lett. **106**, 194502 (2011).
[24] B. Jha, L. Cueto-Felgueroso, and R. Juanes, Phys. Rev. Lett. **111**, 144501 (2013).
[25] C.-Y. Chen, Y.-C. Huang, Y.-S. Huang, and J. A. Miranda, Phys. Rev. E **92**, 043008 (2015).
[26] A. De Wit, Phys. Rev. Lett. **87**, 054502 (2001).
[27] Y. Nagatsu, Y. Ishii, Y. Tada, and A. De Wit, Phys. Rev. Lett. **113**, 024502 (2014).
[28] F. Haudin, J. H. E. Cartwright, F. Brau, and A. de Wit, Proc. Natl. Acad. Sci. U.S.A. **111**, 17363 (2014).
[29] J. W. Cahn and J. E. Hilliard, J. Chem. Phys. **28**, 258 (1958).
[30] A. A. Wheeler, W. J. Boettinger, and G. B. McFadden, Phys. Rev. E **47**, 1893 (1993).
[31] A. Karma, Phys. Rev. Lett. **87**, 115701 (2001).
[32] W. J. Boettinger, J. A. Warren, C. Beckermann, and A. Karma, Annu. Rev. Mater. Res. **32**, 163 (2002).
[33] R. Folch and M. Plapp, Phys. Rev. E **72**, 011602 (2005).
[34] D. M. Anderson, G. B. McFadden, and A. A. Wheeler, Annu. Rev. Mater. Res. **30**, 139 (1998).
[35] R. Folch, J. Casademunt, A. Hernández-Machado, and L. Ramirez-Piscina, Phys. Rev. E **60**, 1724 (1999).
[36] R. Folch, J. Casademunt, A. Hernández-Machado, and L. Ramirez-Piscina, Phys. Rev. E **60**, 1734 (1999).
[37] A. Hernández-Machado, M. Lacasta, E. Mayoral, and E. Corvera-Poiré, Phys. Rev. E **68**, 046310 (2003).
[38] H.-G. Lee, J. S. Lowengrub, and J. Goodman, Phys. Fluids **14**, 492 (2002).
[39] H.-G. Lee, J. S. Lowengrub, and J. Goodman, Phys. Fluids **14**, 514 (2002).
[40] Y. Sun and C. Beckermann, Physica D **237**, 3089 (2008).
[41] L. Cueto-Felgueroso and R. Juanes, Phys. Rev. Lett. **108**, 144502 (2012).
[42] L. Cueto-Felgueroso and R. Juanes, Phys. Rev. Lett. **101**, 244504 (2008).
[43] P. Hohenberg and B. Halperin, Rev. Mod. Phys. **49**, 435 (1977).
[44] S. M. Allen and J. W. Cahn, Acta Metall. **27**, 1085 (1979).
[45] G. Wilson, J. Am. Chem. Soc. **86**, 127 (1964).
[46] T. P. Witelski, Stud. Appl. Math. **97**, 277 (1996).
[47] C. T. Tan and G. M. Homsy, Phys. Fluids **6**, 1330 (1988).
[48] A. Riaz and E. Meiburg, J. Fluid Mech. **494**, 95 (2003).
[49] A. L. Bertozzi, N. Ju, and H.-W. Lu, J. Discrete Continuous Dyn. Syst. **29**, 13671391 (2011).
[50] See supplementary material.
[51] I. M. Lifshitz and V. V. Slyozov, J. Phys. Chem. Solids **19**, 35 (1961).
[52] C. Wagner, Z. Electrochem. **65**, 581 (1961).
[53] J. H. Yao, K. R. Elder, H. Guo, and M. Grant, Phys. Rev. B **47**, 14110 (1993).
[54] D. Fan, S. P. Chen, L. Q. Chen, and P. W. Voorhees, Acta Mater. **50**, 1895 (2002).
[55] C.-Y. Chen and E. Meiburg, J. Fluid Mech. **326**, 57 (1996).
[56] C. Y. Chen, L. Wang, and E. Meiburg, Phys. Fluids **13**, 2447 (2001).